frontiers | Frontiers in Earth Science

TYPE Original Research
PUBLISHED 19 August 2022
DOI 10.3389/feart.2022.906923

OPEN ACCESS

EDITED BY
Hongyuan Liu,
University of Tasmania, Australia

REVIEWED BY
Mingjing Lu,
SINOPEC, China
Shu Longyong,
China Coal Research Institute, China

*CORRESPONDENCE
Xiao Liu,
liuxiao@hpu.edu.cn

SPECIALTY SECTION
This article was submitted to Geohazards and Georisks, a section of the journal Frontiers in Earth Science

RECEIVED 29 March 2022
ACCEPTED 27 June 2022
PUBLISHED 19 August 2022

CITATION
Liu X, Jing T, Lin H, Xuan D, Li Y and Xu S (2022), Morphological characteristics and permeability evolution of deep mine gas drainage boreholes.
Front. Earth Sci. 10:906923.
doi: 10.3389/feart.2022.906923

Morphological characteristics and permeability evolution of deep mine gas drainage boreholes

Xiao Liu[1]*, Tianxiang Jing[1], Haixiao Lin[1], Dequan Xuan[2], Yong Li[1] and Sen Xu[1]

[1]Henan Polytechnic University, Jiaozuo, China, [2]Ventilation Department of Henan Dayou Energy Co. Ltd, Yima, China

Structural coal has low permeability and high gas content. The increase of mining depth seriously restricts the safe mining of deep mines. Hydraulic flushing is the main means of gas extraction. The shape of the hydraulic flushing hole is an important basis to determine the pumping radius, which is widely regarded as a cylinder. However, due to the differences in the stress level, water force, friction and external moisture, the pore morphology, and permeability evolution need to be further studied. At present, the hole shape for hydraulic punching is equivalent to a cylinder in drilling design and evaluation, which is one of the important bases to determine the effective extraction radius. However, the hole shape is affected by many factors, so the scientific equivalent to a cylinder remains to be discussed. The BR-PKN equation describing the hole shape is established by introducing and combining the Bergmark–Roos equation and PKN model, and the hole's shape is shown by MATLAB. To verify its accuracy, YZD18.5 is used as an onsite logging tool for data acquisition and analysis, and the hole section is drawn. The BR-PKN equation and permeability evolution model are simulated by COMSOL Multiphysics, and the permeability evolution law of conventional cylinder with hydraulic flushing is compared and analyzed. The results show that 1) the shape of the hydraulic punch hole is ellipsoid with three different axes, and its horizontal section is approximately an ellipse; 2) within the influence range of quasi-ellipsoid holes, the permeability changes in the long and short axis of quasi-ellipsoid holes are similar. The permeability evolution curve of the coal first increases, then decreases, and finally, flattens with the increase of distance from borehole, and the permeability of the coal body increases with the extension of extraction time); 3) the permeability of the equivalent ellipsoid pore decreases with the increase in coal water content. The effective radius in the long and short axes of the minimum cross section of the quasi-ellipsoid hole is 0.89 and 0.95 times the effective extraction radius of the equivalent cylinder, which provides a basis for a drilling layout.

KEYWORDS

hydraulic flushing, hole shape, the moisture content, numerical simulation, extraction of radius

1 Introduction

After a long period of intense tectonic activity, coal is primarily formed after extrusion, shear deformation, and cohesion of low strength and low permeability. With the increase in mining depth, the distribution of tectonic coal tends to expand. Unloading is a deep mine gas disaster management technology. Hydraulic punching is a tectonic coal unloading extraction gas effective technique, and its role is mainly reflected in the following three aspects (Wu et al., 2002; Wang et al., 2013; Jiang et al., 2018; Liu and Liu, 2019; He et al., 2021): 1) high-pressure water is used to break the coal body, forming a certain range of pressure relief area around the hole, in which the permeability increases substantially, so as to achieves the purpose of gas extraction; 2) wetting coal reduces its elastic potential energy; and 3) water lock reduces gas desorption speed. The pore shape is a key influencing factor in the design of gas drainage. Scholars generally regard the process of hydraulic flushing as a uniform pore expansion, that is, a cylinder with regular pore shape (Wei et al., 2014; Yang et al., 2018; Ren, 2019). However, after flushing, the stress state of the coal body around the hole will change, and the shape of the hole will change correspondingly under the influence of stress, which is not a regular cylinder, thus affecting the gas extraction design.

External moisture is an important part of coal. When external moisture enters coal, it will affect the permeability characteristics and structure of the coal. After hydraulic flushing, the external moisture of the coal around the hole changes, and the permeability of coal will also change under the influence of external moisture. To explore the relationship between water and coal reservoir permeability, many scholars have carried on fruitful research. For example, Jianping Wei conducted independent research and development of the gas coal and rock triaxial seepage test system, determination of coal sample under different moisture content and confining pressure and gas pressure combination of seepage flow, moisture content, and the relationship between the coal containing gas permeability characteristics of expression (Yuan et al., 2015). Li et al.(2020) established a coal-rock permeability model considering the comprehensive effect of water content and fracture compressibility and analyzed the response mechanism of effective compressibility coefficient and permeability of coal rock under different water content conditions. Hao et al. (2016) explored hydraulic flushing around coal gas migration rule and established a creep-under the coupled action of seepage flow hydraulic flushing on the surrounding coal permeability dynamic evolution model, and their results show that hydraulic flushing measures can greatly improve the permeability of the coal body around drilling and coal permeability depending on the space distance, which can quickly reduce the negative power function relationship. On the basis of studying the process of hydraulic flushing and hole shape, this paper studies the hole shape produced by hydraulic flushing and the evolution of coal permeability around the pore with time by means of theoretical analysis and numerical simulation. The results can provide a theoretical basis for the design of mine gas extraction and data support.

2 Methods

2.1 Establishing a hole shape equation for hydraulic flushing

Bergmark–Roos ore drawing theory establishes a mathematical model of loose ore and rock flow from the mechanical point of view. It is assumed that ore and rock particles move continuously from the initial position to the ore drawing port in the shortest distance. The relationship between the gravity of ore and the direct friction of surrounding particles is analyzed from the force of particles in the movement, and the formation principle of ore drawing ellipsoid is clarified. This is a significant development in ore drawing theory research (Ma et al., 2016; Tao et al., 2010; Melo et al., 2007; Kuchta, 2002; Zhang et al., 2019; Liu et al., 2020). The maximum and minimum horizontal principal stresses are the key factors affecting the shape of hydraulic flushing holes. In the horizontal section of the hole after hydraulic flushing, coal and rock are regarded as elastic and brittle materials, the height of the hole is fixed, and the force of water is a constant, which is highly consistent with the PKN model (Tao, 2009; Garikapati et al., 2019; Zheng et al., 2019). In this study, based on the characteristics of coal extraction by water jet and the influence of horizontal stress, the Bergmark–Roos and PKN models were used to establish the shape equation of hydraulic flushing. The BR-PKN equation is as follows:

$$s = \frac{H}{1 - \cos \alpha_G} (\cos \alpha - \cos \alpha_G), \tag{1}$$

where s is the moving distance of particles, m; H is the height of ore body, m; α is the angle between the particle moving trace and the vertical direction, °; and α_G is the maximum angle of dispersion movement, which is determined by the following formula:

$$\alpha_G = 45 - \varphi_0/2, \tag{2}$$

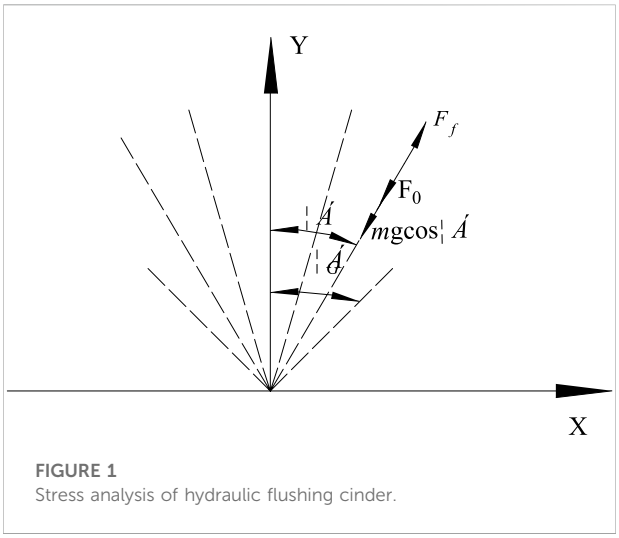

FIGURE 1
Stress analysis of hydraulic flushing cinder.

where φ_0 is the internal friction angle of particles, which changes with particle size and particle roughness. The coarser the particles, the greater the value.

The stress analysis of hydraulic punching coal cinder is shown in Figure 1.

The resultant force F of each component force on coal cinder along the trajectory direction of coal cinder production is

$$F = mg\cos\alpha + F_0 - F_f,$$

where M is mass of coal and rock bulk, kg; G is the acceleration of gravity, 9.81N/kg; F_0 is the force of punching water on coal cinder, N, constant value; and F_f is the friction force between coal and rock bulk, N. Because F_0 is a constant value, so F_0/m is a constant, let F_0/m = ge, e is a constant.

According to the stress analysis of the horizontal section of the hole, the horizontal section is not regular round, and has long axis and short axis. Its short semi-axis r_1 is

$$r_1 = s\sin\alpha = H\frac{\cos\alpha + e - \cos\alpha_G}{1 + e - \cos\alpha_G}\sin\alpha. \quad (3)$$

Hole height Z is

$$Z = s\cos\alpha = H\frac{\cos\alpha + e - \cos\alpha_G}{1 + e - \cos\alpha_G}\cos\alpha. \quad (4)$$

The long half-axis r_2 of the horizontal section can be obtained by the following formula:

$$r_2 = \frac{QH(1 + e - \cos\alpha_G)\left[2xe^{x^2}\mathrm{erfc}(x) + 2/\sqrt{\pi} - 1\right]}{32\pi C^3\sqrt{\pi t}\sin\alpha(\cos\alpha + e - \cos\alpha_G)}, \quad (5)$$

where Q is the change of hole volume, $Q = H^*\frac{dA}{dt}$, m^3/min; C is the coefficient, taken as 1; t is the movement time of coal and rock bulk; $x = \frac{2C\sqrt{\pi t}}{H}$; and erfc (x) is the error compensation function of x.

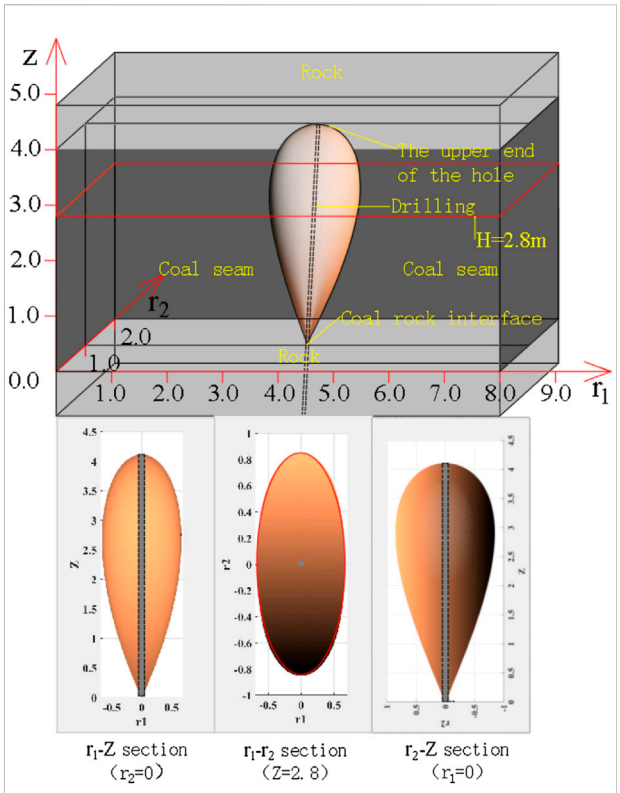

FIGURE 2
Pore morphology and section of hydraulic flushing.

2.2 Drawing of the hole shape equation based on MATLAB

The coal seam thickness of 14250 working face of Xin'an Coal Mine is 0.3–13.1 m, and the average coal thickness is about 4 m. The deduced BR-PKN equation suitable for coal cinder output of hydraulic flushing is displayed in three dimensions by MATLAB, and the shape and section of hydraulic flushing holes are expressed in Figure 2. It is found that the shape of hydraulic flushing holes is a quasi-ellipsoid with a slightly larger top than bottom. The horizontal section of the hole (r_1-r_2 section) is a flat ellipse.

2.3 Field verification of the shape characteristics of hydraulic flushing holes

The hole's shape in hydraulic flushing is restricted by many factors, such as coal-rock bulk gravity, coal-rock friction, water force, stress and so on. Through theoretical derivation, it is found that the hole's shape is ellipsoid-like. To verify the feasibility of BR-PKN equation and verify that the holes' shape is ellipsoid, the hydraulic flushing test was carried out in the cutting bottom plate roadway of

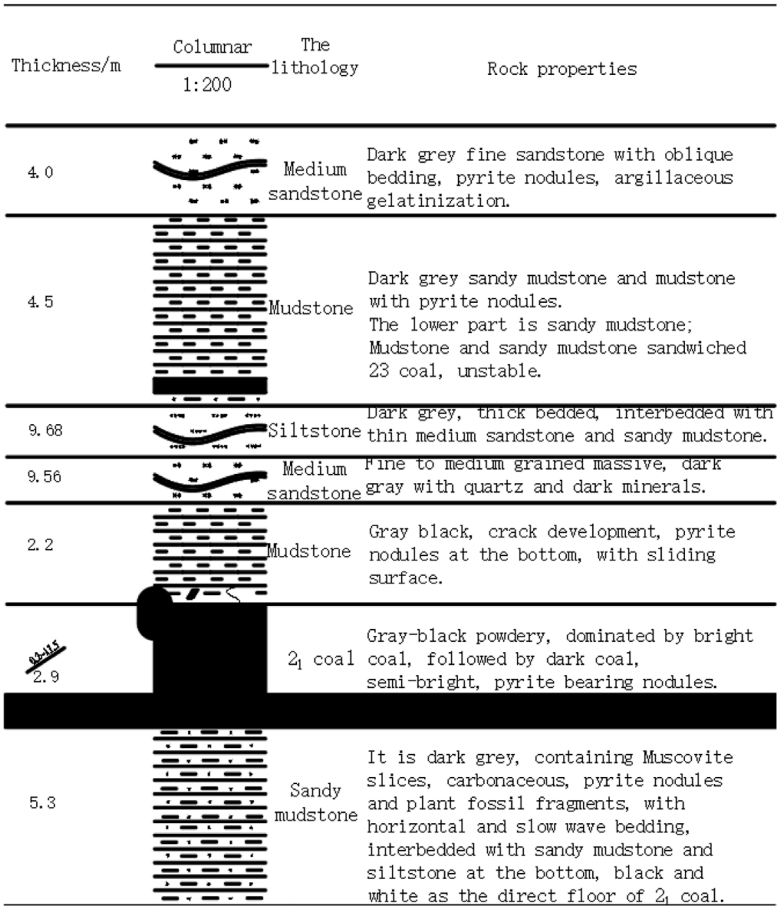

FIGURE 3
Strata histogram of Xin'an Coal Mine.

14250 working face in Xin'an mine. Figure 3 is the stratum bar chart of Xin'an Coal Mine

2.3.1 Test equipment

YZD18.5 mine lateral resistivity video imaging logging tool is mainly composed of a probe, host control box, host control panel, and push rod.

Working principle: select the appropriate detection method according to the demand, then carry out onsite layout and construction, and select the corresponding detection method according to the construction method. The instrument can analyze the rock stratum structure of the borehole through video (e.g., layered lithology, rock hole fracture development, water outlet point characteristics, roof separation, etc.), automatically generate the borehole orientation profile, borehole plane trajectory, and borehole histogram according to the scale through the detection data. There is a camera ahead, which can realize automatic continuous measurement. With the continuous deepening of the push rod in the hole, the instrument can collect parameters such as different hole section diameters and shapes along the hole direction of hydraulic flushing.

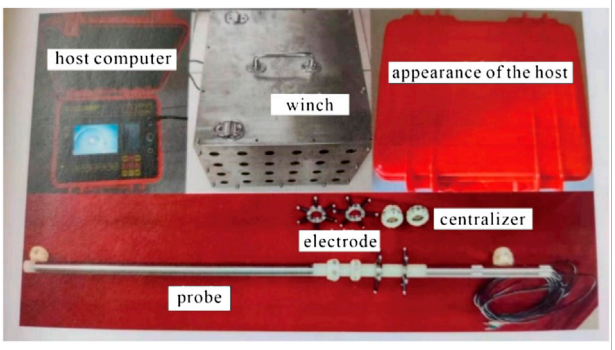

FIGURE 4
YZD18.5 mine lateral resistivity video imaging logging tool.

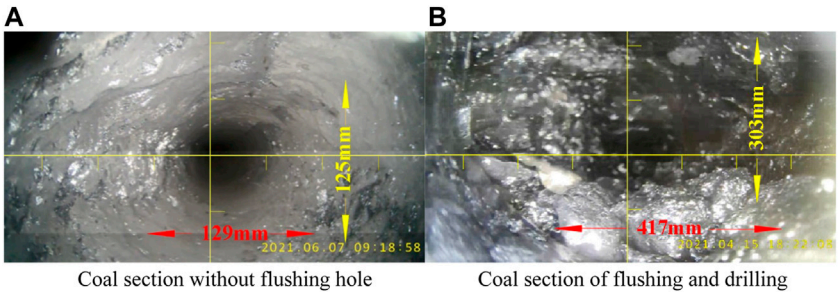

FIGURE 5
Borehole aperture peep view. **(A)** Coal section without flushing hole. **(B)** Coal section of flushing and drilling.

Instrument parameters: the video resolution is 1280 * 960, the probe angle of view is 120°, and the effective sight distance is 300mm; the data acquisition frequency is 15 points/second; the measurement range of borehole inclination is −90° to 90°, and the measurement accuracy is +0.1°; the detection depth is 0–200m, and the hole depth error is less than 0.5%. Figure 4 shows YZD18.5 mine lateral resistivity video imaging logging tool.

2.3.2 Test procedure

1) Select the drill hole after hydraulic flushing, blow out the coal and rock slag in the hole with compressed air to minimize the residue, ensure the smooth drilling, and maintain the drilling shape after hydraulic flushing to the greatest extent
2) The YZD18.5 mine lateral resistivity video imaging logging tool is used for borehole peeping, the collected video files are analyzed, and the standards including acquisition frequency, frequency, and image definition are formulated after many tests
3) The collected image information is summarized and processed in CAD, a section diagram of the hydraulic flushing hole's shape is drawn, and the hydraulic flushing hole's shape is analyzed

2.3.3 Data acquisition and analysis

When the probe of YZD18.5 mining lateral resistivity video imaging logging tool enters the borehole, it is necessary to install the centralizer of corresponding model to ensure that the probe remains in the center of the borehole. The borehole diameter is 113 mm, and the centralizer with diameter of 93 mm is selected. After the probe enters the borehole, it will collect the hole information on the path. When the probe rod reaches the hole bottom and saves the data, the data acquisition is completed.

We then analyze the video files obtained after data acquisition, consider the observation angle of the probe, the effective detection distance of the probe, the forward speed of the probe, the data acquisition frequency and other factors, and use the intercepting frame function on the premise of ensuring the clarity and high accuracy of the image according to the actual test on the site. We plan to collect images every 0.15 m along the hole axis and every 90° along the hole circumference. The gray value of the collected image information is analyzed by schlieren method, the spatial position information contains in the hole section is obtained, and the hole's shape section is drawn, as is shown in Figure 5.

2.3.4 Data processing

Two holes 9-03# and 7-09# are selected to draw the hole morphology diagram, as shown in Figure 6.

In Figure 6, the spatial information of about 40 images was used to draw the sectional map of the cavity morphology. r_1-Z and r_2-Z sections are quasi-ellipsoids with the upper part slightly larger than the lower part and the right-hand side is slightly larger than the left-hand side, and the maximum values of long semi-axis and short semi-axis are obtained at about z = 0.6H. The r_1-r_2 section shows an approximate ellipse, and the values of r_1 and r_2 are close to a constant value. The cross-sectional view of the hole's shape is roughly the same as the three-dimensional display of BR-PKN equation deduced above in MATLAB; that is, the hole's shape after flushing is an ellipsoid with a slightly larger top than the bottom.

2.4 Adsorption-permeability model of coal and rock considering water content

The pore and fissure of coal seam are the main factors affecting the permeability of coal seam, which directly affect the adsorption capacity and permeability characteristics of coal:

$$\varphi = \frac{V_p}{V_b} = \frac{V_{p0} + \Delta V_p}{V_{b0} + \Delta V_b} = 1 - \frac{V_{s0} + \Delta V_s}{V_{b0} + \Delta V_b} = 1 - \frac{1 - \varphi_0}{1 + \varepsilon_v}\left(1 + \frac{\Delta V_s}{V_{s0}}\right), \tag{6}$$

where φ - porosity of coal and rock, %; φ_0 - Initial porosity of coal, %; V_p - volume of coal pore and fissure, and ΔV_p - variation; V_{p0} - initial coal pore fissure volume; V_b - total coal and rock volume, ΔV_b–variation; V_{b0} - initial total coal and rock volume; V_{s0} - coal-

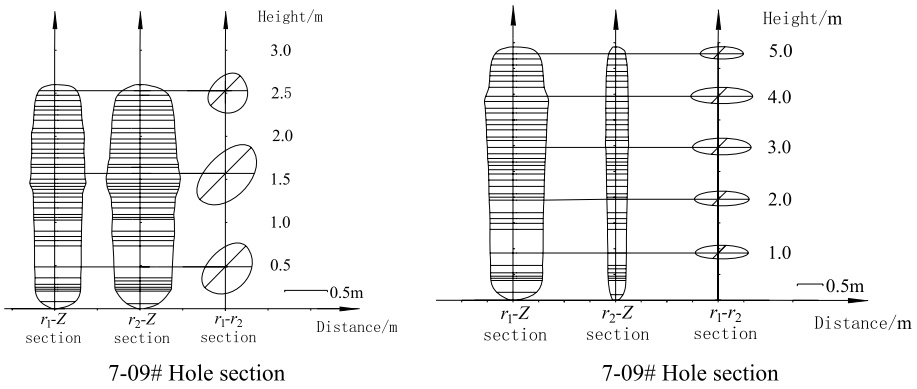

FIGURE 6
Drilling for hydraulic flushing. **(A)** 7-09# hole section. **(B)** 7-09# hole section.

rock skeleton volume; V_s - coal-rock skeleton volume change; and V_ε - Volumetric strain of coal mass.

The internal deformation of coal rock is mainly composed of three parts, which are caused by temperature, gas pressure and adsorption/desorption. Assuming that the temperature of coal and rock is constant, the deformation caused by temperature can be ignored, and only the deformation caused by gas pressure and adsorption/desorption can be expressed as

$$\Delta V_s = -V_{s0}\left(\varepsilon_p - \varepsilon_{sw}\right), \tag{7}$$

where the strain caused by gas pressure ε_p can be expressed as

$$\varepsilon_p = \frac{\Delta p}{K_s}, \tag{8}$$

where Δp- gas pressure change, $\Delta p=p_0-p$, MPa.

Under the condition of uniform surface properties of adsorbents, the adsorption amount of methane in coal and rock was calculated by the Langmuir isothermal adsorption model:

$$V_0 = \frac{abp}{1+bp}, \tag{9}$$

where V_0- gas adsorption capacity (cm^3/g), a- adsorption constant (cm^3/g), b- adsorption constant (MPa^{-1}), and p- gas pressure (Mpa).

When there is water on the surface of coal and rock fissure, there will be adsorption of gas. When the water reaches a certain amount, there will be "water lock effect", which will slow down the release rate of gas and affect the adsorption characteristics of coal and rock (Maggs, 1946; Hu and Wu, 2014). Therefore, the existence of water content should be considered in the establishment of the adsorption model:

$$V = \frac{abp}{1+bp}\exp\left(-\lambda m\right), \tag{10}$$

where V- solid adsorption gas volume (cm^2/g), λ- reduction coefficient of adsorption capacity of coal by humidity, and m- water content (%).

Adsorption deformation of coal rock after adsorption of gas can be obtained by Bangham's theory:

$$\frac{\Delta l}{l} = \gamma\pi, \tag{11}$$

where l- coal-rock width (m), Δl- coal-rock width change value (m), π- surface free energy (J), and γ- deformation constant.

F. A. P. Maggs proposed the relationship between deformation constant and physical and mechanical properties of solids as follows (Tao et al., 2017):

$$\gamma = \frac{\eta\rho_c}{K_s}, \tag{12}$$

where ρ_c- density of coal and rock mass (kg/m^3), η- specific surface area of solid (cm^2), and Ks- adsorption modulus (MPa).

In Gibbs surface adsorption equation, the surface free energy generated by the relative movement between molecules can be described as

$$\pi = RT\int_0^P \Gamma d\left(\ln p\right), \tag{13}$$

where R- Ideal gas constant, Γ- surface excess, and T- temperature (K). When the adsorbed substance is CH_4, the surface excess Γ can be described as

$$\Gamma = \frac{n}{\eta} = \frac{V}{Vm\eta}, \tag{14}$$

where n- total surface excess of adsorbed gas; V_m- molar volume of gas. By substituting Eqs 9, 11–13 into Eq. 12, the linear deformation of coal rock can be obtained as follows:

$$\frac{\Delta l}{l} = \frac{\alpha\rho_c RT}{V_m K_s}\exp(-\lambda m)\int_0^p \frac{bp}{1+bp}dp. \tag{15}$$

Therefore, the adsorption deformation of coal rock is

$$\varepsilon_{sw} = \frac{3\Delta l}{l} = \frac{\alpha\rho_c RT}{V_0 E_A}\exp(-\lambda m)\int_0^p \frac{bp}{1+bp}dp. \tag{16}$$

Substituting Eqs 7, 8, 16 into Eq. 6, the expression of porosity φ can be obtained:

$$\begin{aligned}\varphi &= 1 - \frac{1-\varphi_0}{1+\varepsilon_v}(1-\varepsilon_p+\varepsilon_{sw})\\ &= 1 - \frac{1-\varphi_0}{1+\varepsilon_v}\left[1 - \frac{\Delta p}{K_s} + \frac{3\alpha\rho_s RT}{V_m K_s}\exp(-\lambda m)\ln(1+bp)\right].\end{aligned} \tag{17}$$

The permeability of coal is closely related to its stress state, and the change of stress will lead to the change of coal skeleton and pore volume. Permeability and porosity are closely related. According to the relationship between permeability and porosity,

$$k = \frac{\varphi}{K_Z S_p^2}. \tag{18}$$

Among them,

$$S_p = \frac{A_s}{V_p}, \tag{19}$$

where K- permeability, m^2; K_z- dimensionless constant, value 5; S_p- pore surface area per unit pore volume of coal, cm2; and A_s- total surface area of pores in coal, cm^2. When the permeability changes from the initial state k_0, the porosity can also be re-expressed:

$$\varphi = \frac{V_{p0} + (\Delta V_b - \Delta V_s)}{V_{b0} + \Delta V_{b0}}, \tag{20}$$

$$S_p = \frac{A_{s0}(1+\partial)}{V_{p0} + (\Delta V_b - \Delta V_s)}, \tag{21}$$

where ∂ is the increase coefficient of pore surface area of coal rock, %.

Therefore, the ratio of changed permeability to initial permeability can be obtained:

$$\frac{k}{k_0} = \frac{1}{1+e}\frac{1}{(1+\partial)^2}\left(\frac{V_{p0}+\Delta V_p}{V_{p0}}\right). \tag{22}$$

According to the work of Tao (2009),

$$\frac{V_{p0}+\Delta V_p}{V_{p0}} = 1 + \frac{e}{\varphi_0} - \frac{\Delta V_s}{V_{s0}}\frac{(1-\varphi_0)}{\varphi_0}. \tag{23}$$

Then, the permeability evolution model considering water content can be obtained:

$$k = \frac{1}{1+e}\left[1 + \frac{e}{\varphi_0} + \frac{\Delta P(1-\varphi_0)}{\varphi_0 K_s} - \frac{3\alpha\rho_s RT}{V_m K_s}\exp(-\lambda m)\ln(1+bp)\right]^3. \tag{24}$$

3 Results

3.1 Geometric model and boundary conditions

Xin'an Mine is mainly mined in the Permian coal seam group 1, the thickness of the coal seam is 0.3–13.1 m, the thickness of coal seam is 0.3–13.1 m, the average coal thickness is about 4m, the whole layer soft coal, the firmness coefficient f=0.17, the homogenization is strong, the coal seam density ρ=1400 kg/m^3, the coal seam gas content is 4.0 m^3/t ~14.0 m^3/t, The original gas pressure was 0.4–1.4 MPa, and the coal was extracted by hydraulic flushing technology of the floor roadway through layer, and 1t coal is produced per meter of coal section during hydraulic flushing. Based on this, a numerical calculation geometric model is established, and the maximum punch aperture of the long axis and short axis is 0.76 and 0.63m, respectively. The model parameters are shown in Table 1.

3.2 Permeability evolution of hydraulic flushing coal based on quasi-ellipsoid

During hydraulic flushing, a water jet is used to stimulate coal breaking in a coal seam. During coal breaking, the external moisture of coal seam is increased and the spatial distribution characteristics of permeability of coal body in hydraulic hole are affected. Therefore, the permeability evolution law of coal body under different water bearing conditions is carried out based on the shape of hydraulic flushing hole. COMSOL Multiphysics simulation software was used to simulate the permeability changes of coal body in the long and short-axis directions of equivalent ellipsoid holes and equivalent cylindrical holes at 0, 1, 10, 30, 60 and 90 days after hydraulic drilling under different water cut conditions, on the basis of ellipsoid hole shape, as shown in Figures 7, 8. And Figures 9 shows the comparison of coal permeability along the long and short axes of ellipsoid when water content is 6%. In these figures, the arc length on the abscissa represents the normal distance from the hole (m), and

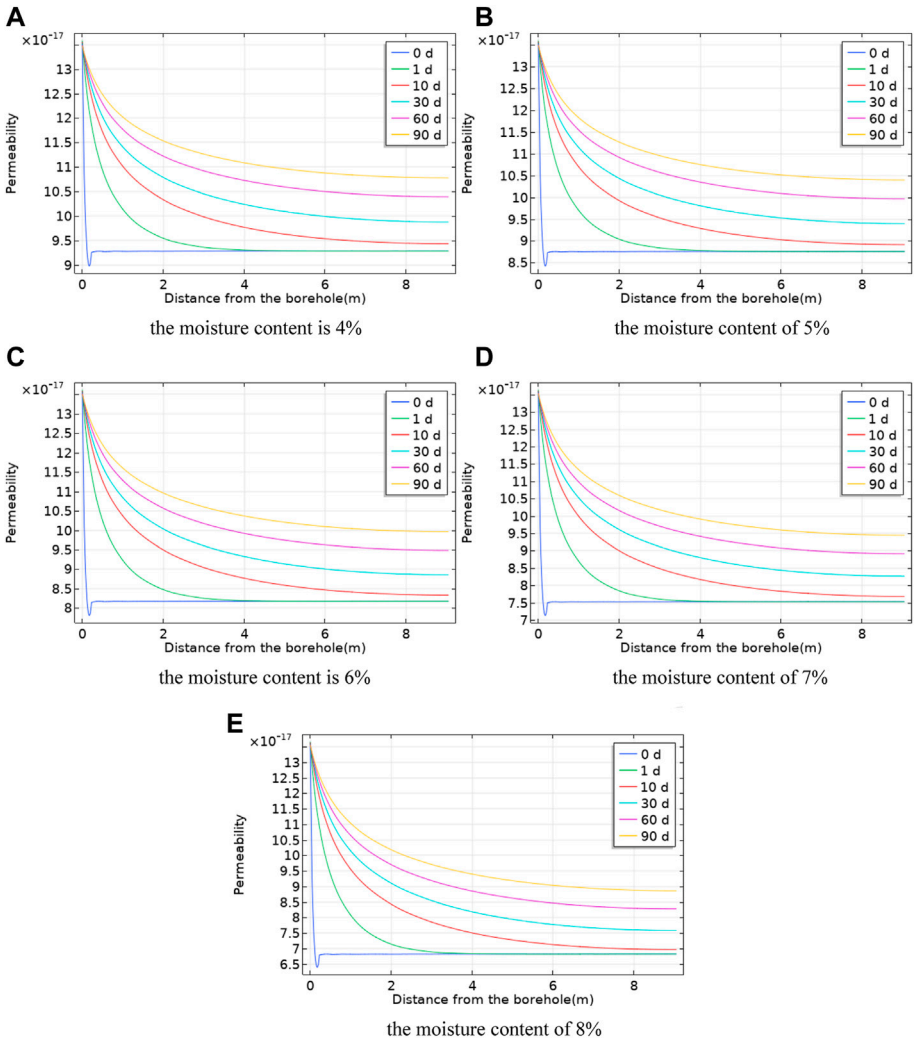

FIGURE 7
Evolution of coal permeability along the long axis of equivalent ellipsoid-like holes under different water content. **(A)** The moisture content is 4%, **(B)** the moisture content is 5%, **(C)** the moisture content is 6%, **(D)** the moisture content is 7%, and **(E)** the moisture content is 8%.

the ordinate represents the permeability of coal around the hole (m^2).

3.2.1 Permeability evolution of the long axis of the equivalent ellipsoidal cavity

According to the permeability curve after hydraulic flushing and the stress state of coal around the hole, the area around hydraulic flushing can be divided into three zones (Hao et al., 2014; Fan et al., 2021). The first is the increased permeability zone; that is, the stress decreased zone, which is 0–2.1 m away from the hole. The coal permeability in this zone increases obviously, and it always exists with the extension of time, and the permeability continues to increase with the extension of time, but the increase rate is small. The second is the decreased permeability zone; that is, the increased stress zone, which is 2.1–6.0 m away from the hole. The permeability of this zone decreases rapidly but it is still larger than the original permeability. Moreover, this zone always exists with the extension of time, and the permeability continues to increase with the extension of time, with a slightly larger increase than that of the increased permeability zone. In the third zone, the permeability flat area, namely the original rock stress area, the distance from the hole is greater than 6.0 m. The stress to the original rock stress in this region is not affected by hydraulic flushing. The penetration of the area gradually overcomes the original permeability, the change is very small with the extension of time, and there is a small increase of permeability.

As can be seen from Figure 7, with the same water content, the coal permeability along the long axis of the equivalent ellipsoid hole shows a trend of uniform growth with the extension of extraction time. With the increase of the distance from the hole, the permeability first increases, then

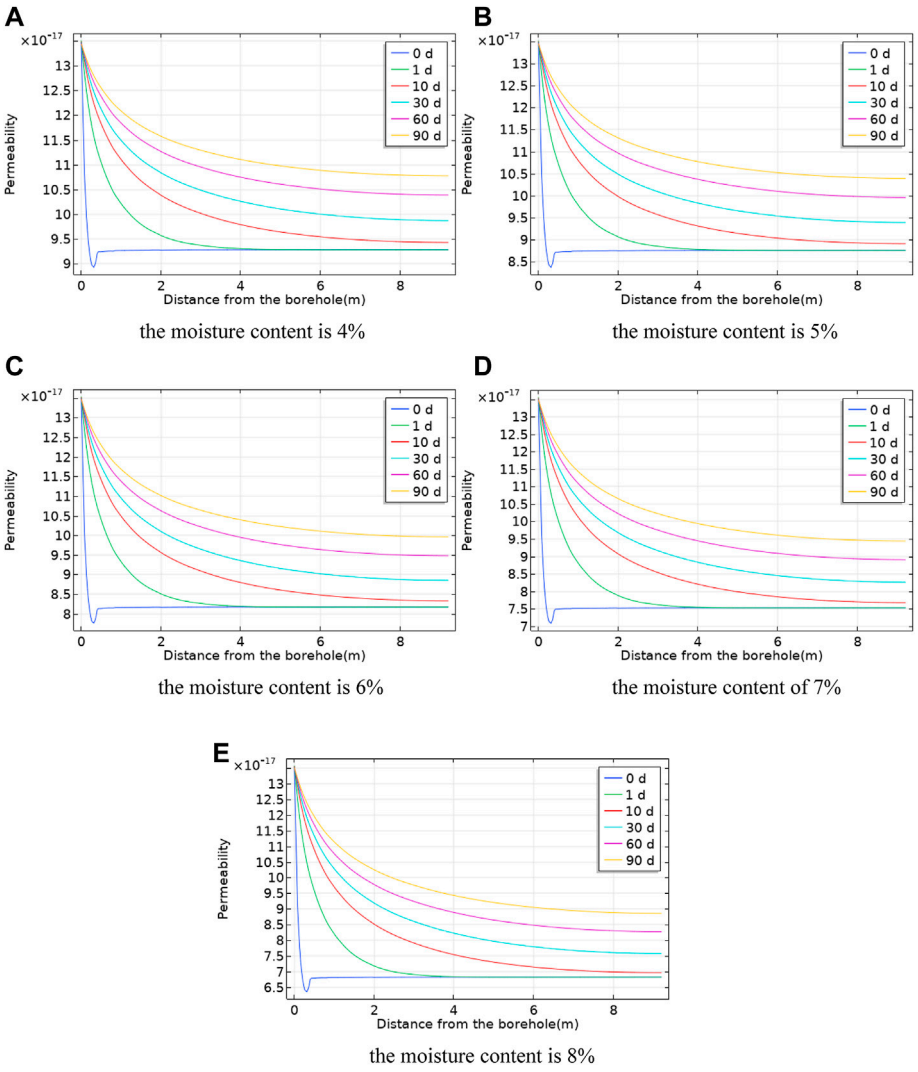

FIGURE 8
Evolution of coal permeability along the short axis of equivalent ellipsoid-like holes under different water content conditions. **(A)** The moisture content is 4%, **(B)** the moisture content is 5%, **(C)** the moisture content is 6%, **(D)** the moisture content is 7%, and **(E)** the moisture content is 8%.

decreases rapidly, and finally tends to be stable. In 0 days of permeability, with the increase of the distance between holes distance fell sharply, and there is a peak at 0.3 m away from the hole location. Permeability then increases because after the hydraulic flushing there is an increased stress anomaly zone around the hole, the area affected by ground stress and force transmission shifts, and the effective stress increases after the coal by water jet impact by compaction. The porosity of coal becomes smaller, resulting in the decrease of permeability in this area. With the extension of time, the coal body gradually recovers. With the increase of water content, the permeability evolution is basically consistent, but the permeability gradually decreases. When the extraction time is 90 days, the water cut is 4%, 5%, 6%, 7%, and 8%, the maximum permeability is the same, which increases by 23.8% compared with the original permeability. Compared with the original permeability, and the stable permeability decreases by 0.9%, 4.6%, 8.3%, 14.8%, and 19.4%, respectively, compared with the original permeability.

3.2.2 Evolution of coal permeability along the short axis of equivalent ellipsoid

It can be found that the evolution curve of coal permeability along the short axis increases first, then decreases, and finally flattens with the increase of distance from the borehole, which is almost consistent with the

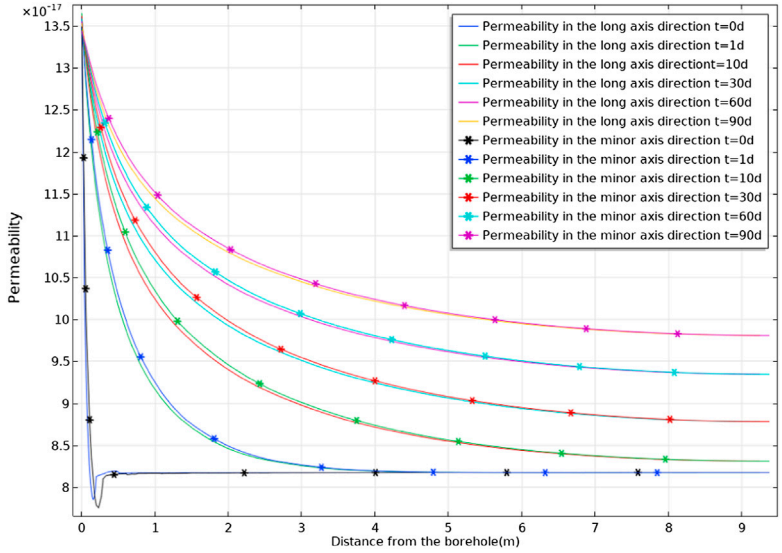

FIGURE 9
Comparison of coal permeability along the long and short axes of ellipsoid when water content is 6%.

permeability along the long axis and slightly smaller in value than that along the long axis.

By observing Figures 7, 8, it can be found that the permeability of coal in the short-axis direction has the following characteristics compared with that in the long-axis direction:

1) The variation law of coal permeability in the short-axis direction of the equivalent ellipsoid hole is roughly consistent with that in the long axis direction.
2) The permeability of the long axis and the short axis changes with the change of stress. The stress value of the long axis and the short axis is almost the same when the distance from the borehole is greater than 4 m, which explains the phenomenon that the evolution curves of the permeability of the long axis same as the short axis when the distance from the borehole is greater than 4 m.

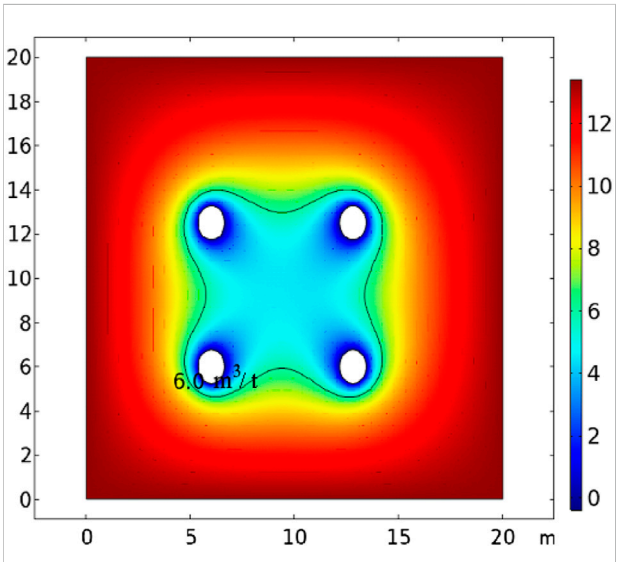

FIGURE 10
Gas content distribution of the maximum horizontal section of the equivalent ellipsoid hole.

3.3 Simulation of the effective radius of hydraulic flushing based on quasi-ellipsoid

COMSOL Multiphysics software was used to simulate the extraction radius of the derived equivalent ellipsoid hole. The area where the gas content is reduced to less than 6 m^3/t is considered as the influence range of effective extraction radius (Li et al., 2011; Wen et al., 2012; Hu et al., 2020; Xu et al., 2020; Xie et al., 2021). COMSOL Multiphysics software was used to set the coal quantity as 1 t/m, the extraction time as 3 months, the spacing of boreholes as 6.60m, and the hole depth as 4.00 m. The drilling sections of equivalent ellipsoid are different. Here, only the maximum and minimum horizontal sections are analyzed. The minimum horizontal section is obtained when it is near the roof and floor of coal seam, and the maximum long axis and short axis are about half of the maximum horizontal section. The

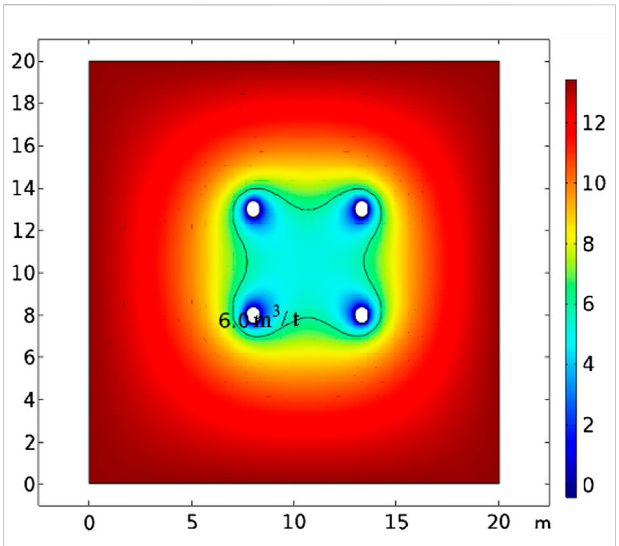

FIGURE 11
Gas content distribution of the minimum horizontal section of the equivalent ellipsoid hole.

maximum horizontal section of short semi-axis r_{1m} and long semi-axis r_{2m} are 0.63 and 0.76 m, respectively, while the minimum section of short semi-axis r_1 and long semi-axis r_2 are 0.315 and 0.38 m, respectively. After 90 days of drainage, the gas content distribution around the borehole is shown in Figures 10, 11.

Figures 10, 11 show the gas content isolines after 90 days of extraction, and areas below the isolines of 6 m^3/t are regarded as effective extraction ranges. It is found that the maximum effective extraction radius of the equivalent ellipsoid hole is 3.25 m in the long-axis direction and 3.40 m in the short-axis direction. The minimum effective extraction radius in the long-axis direction of the cross-section is 2.50 m and the effective extraction radius in the short-axis direction is 2.65 m.

3.4 Comparison of ellipsoid-like and cylindrical holes

3.4.1 Permeability correlation

Figure 12 shows the moisture content of 6% when the equivalent of evolution of coal permeability curves around the cylinder holes. When the moisture content is 6%, the coal permeability of two horizontal directions are perpendicular to each other, which in the equivalent cylinder showed a uniform growth trend. With the increase of the distance from the hole, the permeability first increases, after rapidly decreases, and finally tends to be stable. With the increase of water content, the permeability evolution is basically consistent, but the permeability gradually decreases. At 90 days of extraction, the maximum permeability at a water cut of 6% increased by 23.8% compared to the original permeability and the stationary permeability decreased by 10.6% compared to the original permeability.

Figure 13 shows the evolution curve of coal permeability around the quasi-ellipsoid hole and cylindrical hole with different distances from the hole under the condition of 6% water content. The dotted

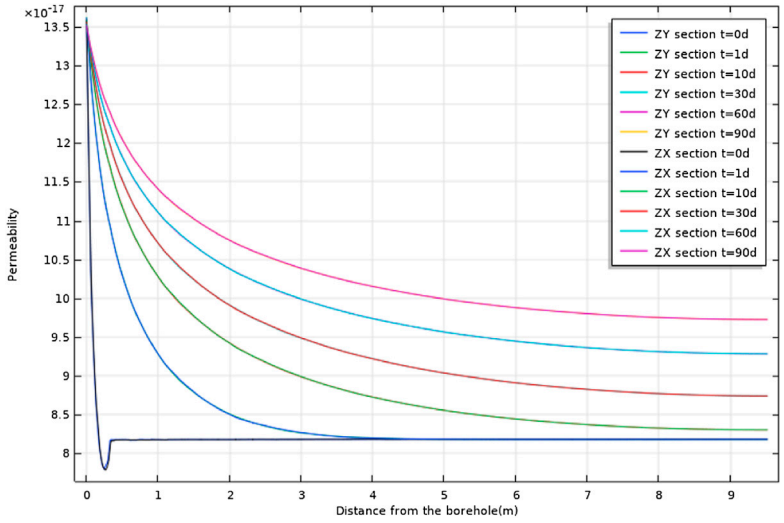

FIGURE 12
Permeability evolution of coal around cylinder hole when water content is 6%.

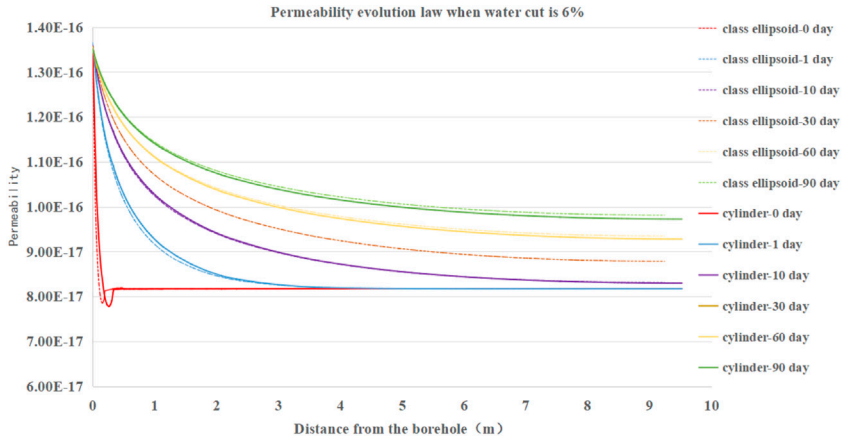

FIGURE 13
Permeability evolution under different pore morphology when water content is 6%.

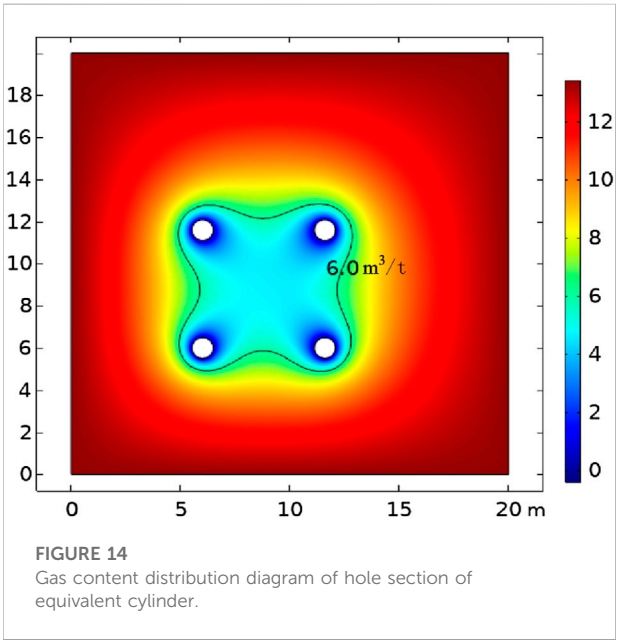

FIGURE 14
Gas content distribution diagram of hole section of equivalent cylinder.

line in the figure represents the evolution law of coal permeability around the equivalent quasi-ellipsoid hole, and the solid line represents the permeability and evolution law around the equivalent cylindrical hole. By comparing the permeability curves of the two holes, it can be found that

1) The permeability evolution of the two pore shapes has the same change trend with water content, and both of them show that the permeability decreases with the increase of water content
2) When the time is the same, the water content is 6% and the coal output is 1 t/m, the permeability of coal around the long axis of the equivalent ellipsoid hole is less than that of the equivalent cylinder hole within 0–30 days after flushing, and that of coal around the long axis of the equivalent ellipsoid hole is greater than that of the equivalent cylinder hole during 60–90 days

3.4.2 Comparison of effective extraction range

Figure 14 shows the gas content distribution diagram of the section of the equivalent cylinder hole. It can be found that the effective drainage radius of the equivalent cylinder hole by hydraulic flushing is 6.6 m after 90 days of drainage. A comparison with Figures 10, 11 shows that

1) The maximum effective extraction radius of the quasi-ellipsoid hole in the longitudinal direction is 1.16 times that of the equivalent cylindrical hole, and the effective extraction radius in the short-axis direction is 1.21 times that of the cylindrical hole
2) The effective extraction radius of the minimum section of the quasi-ellipsoid in the long-axis direction is 0.89 times that of the equivalent cylinder, and the effective extraction radius in the short-axis direction is 0.95 times that of the cylinder

This suggests that in the actual hole pattern for the class under the condition of ellipsoid, an equivalent cylinder hole arrangement is not reasonable in the evaluation of extraction of prone to extraction standards. However, the existence of blank tape, ellipsoid to class hole of radius of the cross-section of short axis efficient extraction-based layout borehole can effectively avoid extraction of white space, improve the effect of the gas extraction, and ensure the safety of mine production.

TABLE 1 Numerical model parameters.

Parameter	Initial porosity /%	Initial porosity/m^2	Poisson's ratio of coal	The coefficient of Klinkenberg a/MPa	Adsorption constant a/ (m^3/t)	Adsorption constant b/ MPa^{-1}	The temperature /K
The values	0.0494	1.09*10-16	0.32	0.76	32	0.72	293
Parameter	The density of coal rho/(t/m^3)	Modulus of elasticity E/GPa	Elastic modulus of solid skeleton Ks/GPa	Initial gas pressure /MPa	Atmospheric pressure /kPa	Initial gas density /(kg/m^3)	
The values	1.40	2.20	3.20	1.40	101	0.716	

TABLE 2 Hydraulic flushing drilling parameters.

Borehole no.	Dip angle(°)	Hole depth /m	Length of coal section H/m	Actual coal output /t	Calculated coal quantity /t	Calculation of the maximum long half-axis r_1/m	Calculation of the maximum minor axle r_2/m
9-03	34	14.40	2.60	1.40	0.53	0.42	0.51
7-09	72	18.80	4.90	4.20	3.42	0.79	0.94
12-12	35	31.80	5.40	6.30	4.59	0.87	1.04
16-05	44	26.00	6.60	7.56	8.50	1.07	1.29
11-09	75	20.00	7.20	10.50	11.33	1.13	1.42

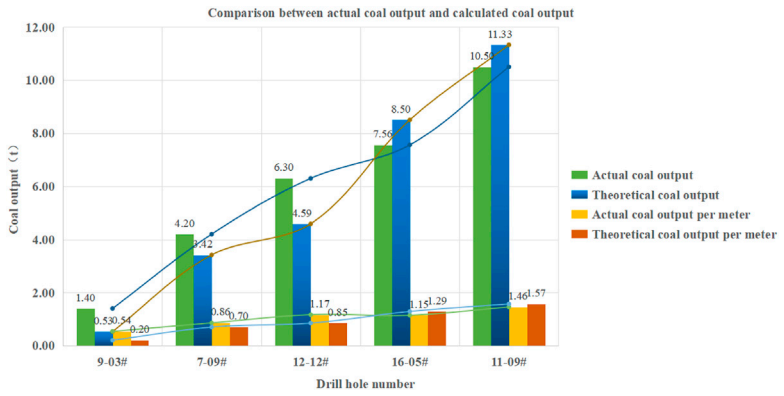

FIGURE 15
Comparison between actual coal output and calculated coal output.

3.5 Test data analysis

After the test, boreholes with different coal thicknesses in the bottom roadway at 14250 working face were selected to collect drilling parameters of hydraulic punching. The specific drilling parameters are shown in Table 2.

In Table 2, coal extraction volume is composed of coal extraction volume from hydraulic flushing and coal extraction volume from drilling. By substituting test data into Eq. 5, parameters b=0.04 and α_G=18° are fitted. Figure 15 shows the comparison between the actual coal output and the calculated coal output.

As can be seen from Figure 15, with the increase of coal thickness from the borehole, the coal output presents a rising trend, and the average coal output per meter increases with the increase of coal thickness. The coal thickness of hole 9-03# is 2.60m, and the actual average coal output is 0.54 t/m. The coal thickness of hole 11-09# is 7.60m, and the actual average coal yield is 1.46 t/m; that is, the average coal yield from hole 11-09 increases with the increase of coal thickness. The calculated maximum short-axis r_1 and long-axis r_2 of the hole also increased, and the ratio of r_2 to r_1 remained roughly at about 1.20.

4 Conclusion

1) For the shape of the hole after hydraulic flushing, the BR-PKN equation was established by combining the Bergmark–Roos equation and the PKN model, and the numerical simulation was carried out. The shape of the hole was displayed in MATLAB in three dimensions, and it was found that the shape of the hole was a quasi-ellipsoid with the upper part slightly larger than the lower part and the horizontal section approximately elliptic.
2) When the water content is constant, the permeability of coal around the equivalent ellipsoid hole increases gradually with time. With the increase of the distance from the hole, the permeability increases first, then decreases rapidly, and finally tends to be stable. When the water content increases, the permeability of coal generally decreases, which indicates that the increase of coal external moisture will inhibit the permeability characteristics of coal seam.
3) When the water content is 6%, and the coal output is 1 t/m, the permeability of coal around the long axis of the equivalent ellipsoid hole is less than that of the equivalent cylinder hole in 0–30 days after flushing, and it is greater than that of the equivalent cylinder hole in 60–90 days.
4) When the extraction time is 90 days and the water content is 6%, the effective extraction radius of the minimum section of quasi-ellipsoid is 2.50 m along the long axis and 2.65 m along the short axis, which are 0.89 and 0.95 times of the hydraulic hole of equivalent cylinder, respectively. Combined with the above data, it is necessary to optimize the spacing of extraction holes. It is recommended that the spacing of drilling rows be 5.00 m (direction of maximum horizontal principal stress) and 5.30 m (direction of minimum horizontal principal stress).
5) The present study is in the vertical coal layers of drilling on the basis of research on the hydraulic flushing holes form. However, in practice the hydraulic flushing hole shape is affected by factors such as the dip angle of the coal seam and borehole inclination. These factors need further multi-factor coupling under the condition of hole shape characteristic research to optimize the extraction from drilling and to provide theoretical basis for design and evaluation.

Data availability statement

The original contributions presented in the study are included in the article/Supplementary Material; further inquiries can be directed to the corresponding author.

Author contributions

TJ and SX contributed to the writing of the manuscript. DX and YL made a contribution to the field work. XL and HL revised the manuscript. All authors have read and agreed to the published version of the manuscript.

Funding

This study was supported by the Youth Project of National Natural Science Foundation of China (51804100).

Acknowledgments

The authors thank Zhifeng Zhang, Lisheng Zhang, and the other personnel in the field test of the Xin'an Coal Mine for their help.

Conflict of interest

Author DX is employed by Ventilation Department of Henan Dayou Energy Co., Ltd.

The remaining authors declare that the research was conducted in the absence of any commercial or financial relationships that could be construed as a potential conflict of interest.

Publisher's note

References

Fan, Y. P., Shu, L. Y., Huo, Z. G., Hao, J. W., and Li, Y. (2021). Numerical simulation of sectional hydraulic reaming for methane extraction from coal seams. *J. Nat. Gas Sci. Eng.* 95, 104180. doi:10.1016/j.jngse.2021.104180

Garikapati, Hasini, Verhoosel, Clemens V., Harald van Brummelen, E., Zlotnik, S., and Pedro, D. (2019). Sampling-based stochastic analysis of the PKN model for hydraulic fracturing. *Comput. Geosci.* 23 (1), 81–105. doi:10.1007/s10596-018-9784-y

Hao, F. C., Sun, L. J., and Liu, M. J. (2014). Research on boreholes space optimization of hydraulic flushing considering press relief and gas drainage effect. *J. Min. Saf. Eng.* 31 (05), 756–763. doi:10.13545/j.issn1673-3363.2014.05.015

Hao, F. C., Sun, L. J., and Zhao, F. J. (2016). Research on coal permeability spatio-temporal evolution around hydraulic flushing based on creep-seepage coupling. *J. Saf. Sci. Technol.* 12 (08), 16–22. doi:10.11731/j.issn.1673-193x.2016.08.003

He, L. W., Dai, Y. C., Xue, S., Zheng, C. S., Han, B. Q., Guo, X., et al. (2021). Study on gas control methods optimization for mining safety. *Adv. Civ. Eng.* 1, 1. doi:10.1155/2021/4594330

Hu, K., Xia, B. W., Liu, C. W., Lu, Y. Y., and Song, Z. Y. (2020). Effective methane extraction radius after high-pressure water jet slotting. *Geofluids* 1, 1. doi:10.1155/2020/8820540

Hu, Y. L., and Wu, X. M. (2014). Research on coalbed methane reservoir water blocking damage mechanism and anti-water blocking. *J. China Coal Soc.* 39 (06), 1107–1111. doi:10.13225/j.cnki.jccs.2013.1024

Jiang, J. Y., Yang, W. H., Cheng, Y. P., Lv, B. M., Zhang, K., Zhao, K., et al. (2018). Application of hydraulic flushing in coal seams to reduce hazardous outbursts in the mengjin mine, China. *Environ. Eng. Geoscience* 24 (4), 425–440. doi:10.2113/eeg-2110

Kuchta, M. E. (2002). A revised of the Bergmark-Roos equation for describing the gravity flow of broken rock. *Min. Res. Eng.* 11 (4), 349–360. doi:10.1142/s0950609802001002

Li, B. B., Cheng, Q. Y., Li, J. H., Wang, B., and Xu, J. (2020). Study on fracture compression and permeability of water-bearing coal. *Chin. J. Rock Mech. Eng.* 39 (10), 2069–2078. doi:10.3390/app9122549

Li, B., Liu, M. J., Liu, Y. W., Wang, N. H., and Guo, X. L. (2011). Research on pressure relief scope of hydraulic flushing bore hole. *Procedia Eng.* 26, 382–387. doi:10.1016/j.proeng.2011.11.2182

Liu, D., and Liu, W. (2019). Research on gas extraction technology: Hydraulic stamping and hydro fracture to pressure relief and permeability improvement. *Coal Sci. Technol.* 47 (3), 136–141. doi:10.1016/j.jngse.2019.103067

Liu, Y. M., Wang, C. H., and Zhou, H. (2020). Optimization scheme of hydraulic fracturing simulation experiments using mixed-level uniform design method based on the PKN model. *J. Phys. Conf. Ser.* 1, 012165. doi:10.1088/1742-6596/1574/1/012165

Ma, G., Liu, X., and Li, F. (2016). Study on morphology features of hydraulic flushing hole based on ore drawing theory. *Coal Sci. Technol.* 44 (11), 73–77. doi:10.13199/j.cnki.cst.2016.11.014

Maggs, F. A. P. (1946). The adsorption-swelling of several carbonaceous solids. *Trans. Faraday Soc.* 42, B284–B288. doi:10.1039/TF946420B284

Melo, F., Vivanco, C., Fuentes, C., and Apablaza, V. (2007). On drawbody shapes: From Bergmark–Roos to kinematic models. *Int. J. Rock Mech. Min. Sci.* 44 (1), 77–86. doi:10.1016/j.ijrmms.2006.04.010

Ren, Z. J. (2019). Application of hydraulic punching technology in seam gas drainage in yuwu coal mine. *Coal Eng.* 51 (03), 65–70.

Tao, G. Q., Yang, S. J., Liu, Z. D., and Ren, Q. Y. (2010). Research of ore drawing method of broken ore and rock based on Bergmark-Roos equation. *J. China Coal Soc.* 35 (05), 750–754. doi:10.1016/S1876-3804(11)60004-9

Tao, Y. Q., Feng, D., Ma, G., Xu, J., and Peng, S. J. (2017). Study on physical simulation experiment of hydraulic borehole flushing and pressure released and permeability improved effect. *Coal Sci. Technol.* 45 (06), 55–60. doi:10.13199/j.cnki.cst.2017.06.009

Tao, Y. Q. (2009). *Study on the gassy coal THM coupling model and coal and gas outburst simulation[D]*. China: Chongqing University.

Wang, K., Li, B., Wei, J. P., and Li, P. (2013). Change regulation of coal seam permeability around hydraulic flushing borehole. *J. Min. Saf. Eng.* 30 (05), 778–784.

Wei, J. P., Wei, L., and Wang, D. K. (2014). Experimental study of moisture content influences on permeability of coal containing gas. *J. China Coal Soc.* 39 (01), 97–103. doi:10.13225/j.cnki.jccs.2013.0209

Wen, Z. H., Wei, J. P., Liu, Y. Z., and Zhang, H. T. (2012). Numerical simulation on effective influence radius of hydraulic flushing borehole. *Adv. Mat. Res.* 616-618, 1021–1026. doi:10.4028/www.scientific.net/amr.616-618.1021

Wu, H. J., Li, X. L., Gao, X., Chen, D. Y., and Li, Z. (2002). Development and application of water sealing technology for gas drainage boreholes. *ACS omega* 7 (1), 733–743. doi:10.1021/acsomega.1c05385

Xie, S. R., Cui, J. Q., Chen, D. D., and Chen, P. (2021). Numerical simulation study on gas drainage by interval hydraulic flushing in coal seam working face. *Energy Explor. Exploitation* 39 (4), 1123–1142. doi:10.1177/01445987211010274

Xu, D. D., Tao, Y. Q., Zhou, Z. T., Hou, C., and Fabio, M. (2020). Study of the law of hydraulically punched boreholes on effective gas extraction radius under different coal outputs. *Shock Vib.* 1, 12. doi:10.1155/2020/8858091

Yang, S., Liu, X. F., Zhang, C., Liu, Q. L., and Gong, C. Z. (2018). Numerical solution of effective radius of hydraulic punching based on klinkenberg effect. *Saf. Coal Mines* 49 (06), 152–155. doi:10.13347/j.cnki.mkaq.2018.06.040

Yuan, L., Lin, B. Q., and Yang, W. (2015). Research progress and development direction of gas control with mine hydraulic technology in China coal mine. *Coal Sci. Technol.* 43 (01), 45–49. doi:10.13199/j.cnki.cst.2015.01.011

Zhang, M. L., Zhang, T. Y., and Fan, J. Y. (2019). Calculation and analysis of fracture extension parameters based on PKN model. *Sci. Technol. Eng.* 19 (5), 116–123.

Zheng, Y. F., Zhai, C., and Ni, G. H. (2019). Study on performance of fracturing fluid based on surfactant releasing water locking effect. *Saf. Coal Mines* 50 (11), 1–5. doi:10.13347/j.cnki.mkaq.2019.11.001